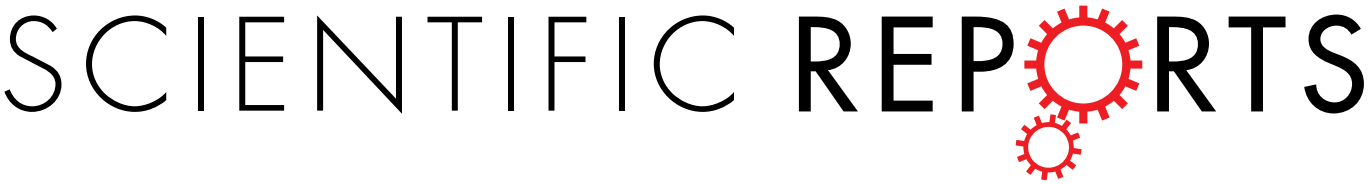

OPEN

Received: 11 January 2015
Accepted: 27 March 2015
Published: 01 June 2015

Giant enhancement in critical current density, up to a hundredfold, in superconducting $NaFe_{0.97}Co_{0.03}As$ single crystals under hydrostatic pressure

Babar Shabbir[1], Xiaolin Wang[1], S. R. Ghorbani[1,2], A. F. Wang[3], Shixue Dou[1] & X.H. Chen[3]

Tremendous efforts towards improvement in the critical current density "J_c" of iron based superconductors (FeSCs), especially at relatively low temperatures and magnetic fields, have been made so far through different methods, resulting in real progress. J_c at high temperatures in high fields still needs to be further improved, however, in order to meet the requirements of practical applications. Here, we demonstrate a simple approach to achieve this. Hydrostatic pressure can significantly enhance J_c in $NaFe_{0.97}Co_{0.03}As$ single crystals by at least tenfold at low field and more than a hundredfold at high fields. Significant enhancement in the in-field performance of $NaFe_{0.97}Co_{0.03}As$ single crystal in terms of pinning force density (F_p) is found at high pressures. At high fields, the F_p is over 20 and 80 times higher than under ambient pressure at12 K and 14 K, respectively, at $P = 1$ GPa. We believe that the Co-doped NaFeAs compounds are very exciting and deserve to be more intensively investigated. Finally, it is worthwhile to say that by using hydrostatic pressure, we can achieve more milestones in terms of high J_c values in tapes, wires or films of other Fe-based superconductors.

Significant advances towards high performing Fe-based superconducting materials (FeSCs) have been made so far, because the combination of reasonable value of critical temperature (T_c), extremely high upper critical field (H_{c2}) on the order of 100 T, high intrinsic pinning potential, low anisotropy (generally between 1-8), and high irreversible field (H_{irr}) makes this class of superconductors particularly attractive for large current and high field applications, where the critical current density (J_c) is a major limiting factor[1–14]. Therefore, improvement in J_c by using various methods has also been one of the most important topics in the superconductivity research field. Texturing procedures, ion implantation/irradiation, and chemical doping are the most common approaches to enhancing J_c in different superconductors. Although J_c values can be improved by these methods, the major drawbacks are that J_c decays rapidly in high fields, especially at high temperatures. Therefore, the J_c values of the Fe-based superconductors at high fields and temperatures need to be improved. Furthermore, T_c and low field J_c deteriorate significantly for various types of superconductors under these approaches, which make them rather impractical for application. The reported enhancement in J_c values at high fields and temperatures is still not more than one order of magnitude.[5,15–22]. Generally, the requirements for enhancing J_c in superconductors

[1]Spintronic and Electronic Materials Group, Institute for Superconducting and Electronic Materials, Australian Institute for Innovative Materials, University of Wollongong, North Wollongong, NSW 2522, Australia. [2]Department of Physics, Ferdowsi University of Mashhad, Mashhad 9177948974, Iran. [3]Department of Physics, University of Science and Technology of China, Hefei, 230026, P. R. China. Correspondence and requests for materials should be addressed to X.W. (email: xiaolin@uow.edu.au)

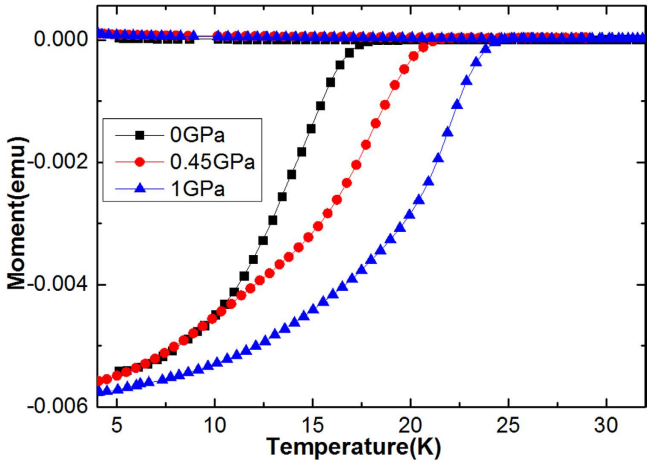

Figure 1. Temperature dependence of magnetic moment at different applied pressures in both ZFC and FC runs for $NaFe_{0.97}Co_{0.03}As$.

include T_c enhancement, which can increase the effective superconducting volume, and the formation of more effective point pinning centres (related to the pinning mechanism).

Hydrostatic pressure has many significant impacts on Fe-based superconductors. For instance, pressure can raise the onset T_c up to 50 K at 1.5 Gpa for $LaFeAsO_\delta$[23]. The application of pressure on $BaFe_{1.92}Co_{0.08}As_2$ results in a very strong enhancement of T_c from 11 to 21 K at 2.5 Gpa[24]. For Co-doped NaFeAs, enhancement in T_c is more than 14 K at 2.5 GPa due to optimization of the structural parameters of the FeAs layers[25]. The T_c of FeSe is enhanced up to 37 K at 7 Gpa[26]. Furthermore, pressure can induce reduction in anisotropy, more effective point pinning centres, and enhancement in T_c. We already anticipated in our previous case study that the most significant approach to enhancing Jc, particularly at high fields and temperatures, without degradation of Tc, is the use of hydrostatic pressure[27].

Most recent research regarding J_c enhancement and pinning mechanisms is mainly focused on the 1111 system (RFeAsO, where R is a rare earth element), the 122 system ($BaFe_2As_2$, $Ba_{0.5}K_{0.5}Fe_2As_2$) and the iron chalcogenide 11 system. Only one report has revealed the nature of the pinning mechanism in LiFeAs (111 type FeSCs) so far, despite its simple structure and reasonable T_c value as compared to the 1111 and 122 types[28]. NaFeAs ($T_c \approx 10$ K) experiences three successive phase transitions around 52, 41 and 23 K, which can be related to structural, magnetic, and superconducting transitions, respectively[29–31]. Bulk superconductivity in NaFeAs with T_c of ~ 20 K can be achieved by the substitution of Co on Fe sites, which can suppress both magnetism and structural distortion[25,32]. The T_c of $NaFe_{0.97}Co_{0.03}As$ single crystal is more sensitive to hydrostatic pressure as compared to other 11 and 111 Fe-based superconductors, and it has a large positive pressure coefficient[25]. In addition, J_c values for Co-doped NaFeAs compounds have not been reported so far. Therefore, it is very interesting to see if the hydrostatic pressure can significantly improve the flux pinning for such compounds. High-quality $NaFe_{0.97}Co_{0.03}As$ single crystals were grown by the conventional high temperature solution growth method using the NaAs self-flux technique[30]. In this communication, we report that hydrostatic pressure can enhance the J_c by more than 100 times at high fields at 12 K and 14 K in $NaFe_{0.97}Co_{0.03}As$ single crystal. This is a giant enhancement of J_c and a record high to the best of our knowledge. The H_{irr} is improved by roughly 6 times at 14 K under $P = 1$ GPa.

The temperature dependence of the magnetic moment for zero-field-cooled (ZFC) and field-cooled (FC) curves at different pressures are shown in Fig. 1. The T_c increases with pressure, from 17.95 K for $P = 0$ GPa to 24.33 K for $P = 1$ GPa, with a huge pressure coefficient, i.e. $dT_c/dP \sim 6.36$ K/GPa, which is nearly same to what we have already reported for $NaFe_{0.97}Co_{0.03}As$ single crystal i.e. $dT_c/dP = 7.06\ K{\cdot}GPa^{-1}$[25]. Interestingly, this pressure coefficient is more than two times greater than that of FeSe ($3.2\ K{\cdot}GPa^{-1}$)[33]. The pressure-induced enhancement of T_c in $NaFe_{0.97}Co_{0.03}As$ can be associated with the optimization of the structural parameters of the FeAs layers, including the As–Fe–As bond angle and anion height[25,34].

The field dependence of J_c at different temperatures obtained from the *M-H* curves by using Bean's model, at $P = 0$ GPa, $P = 0.45$ GPa and $P = 1$ GPa are shown in Fig. 2. Remarkably, J_c is increased significantly at both low and high fields, especially with enhancement of more than 10 times and up to more than 100 times for low and high fields at both 12 and 14 K, respectively. The significant positive effect of hydrostatic pressure on the J_c at high fields and temperatures is further reflected in Fig. 3, which shows the J_c enhancement ratio (i.e. J_c^{1GPa}/J_c^{0GPa}) at 12 and 14 K over a wide range of fields. We have taken the J_c value at $P = 0$ GPa as a reference. The J_c ratio values at both temperatures show significant improvements at low and high fields. Although this result also suggests that hydrostatic pressure is more effective at high fields and temperatures, it is worth mentioning that J_c values are well improved at zero field at a

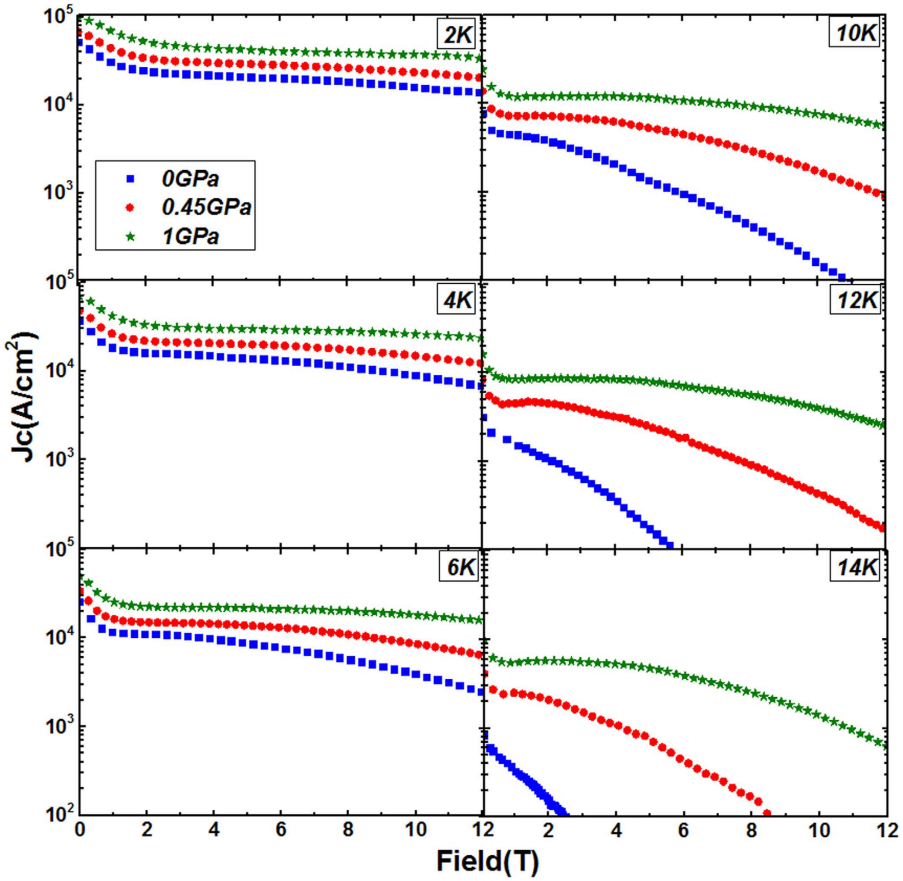

Figure 2. Field dependence of J_c at different pressures (0, 0.45 and 1 GPa) at different temperatures.

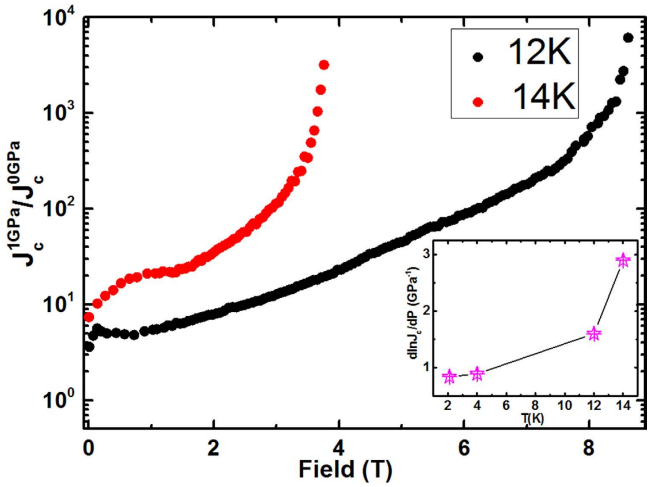

Figure 3. Plot of J_c^{1GPa}/J_c^{0GPa} versus field at 12 K and 14 K. There is a giant enhancement in J_c values at $P = 1$ GPa. The inset shows the plot of $d(\ln J_c)/dP$ versus temperature, which demonstrates enhancement in $\ln J_c$ at a rate of nearly 3 GPa^{-1} at 14 K at zero magnetic field.

significant rate, i.e. $d(\ln J_c)/dP = 1.6$ and 2.9 GPa^{-1} at 12 and 14 K, respectively, as can be seen from the inset of Fig. 3. The $d(\ln J_c)/dP$ values that have been found are more significant than for yttrium barium copper oxide(YBCO)[35].

We also found that H_{irr} of $NaFe_{0.97}Co_{0.03}As$ is significantly increased by pressure. As shown in Fig. 4, the H_{irr} values improve gradually with pressure, and the H_{irr} value at 14 K is increased from 2.6 T at P = 0 GPa up to 8.67 T at P = 0.45 GPa and roughly more than 13 T at P = 1 GPa (by nearly six times).

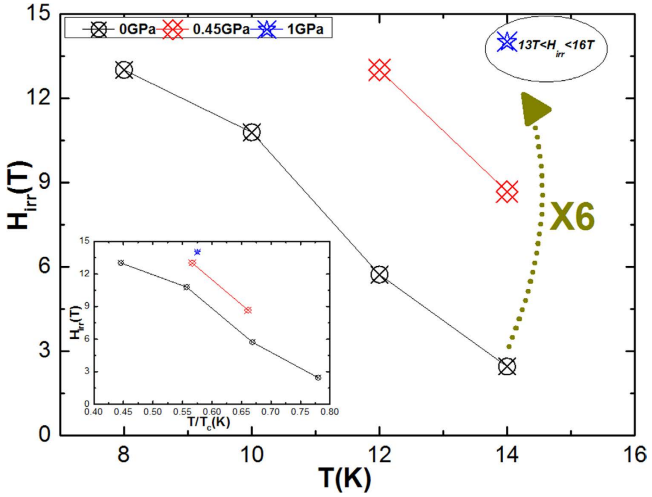

Figure 4. Plot of H_{irr} versus temperature at different pressures. Inset shows H_{irr} as a function of reduced temperature.

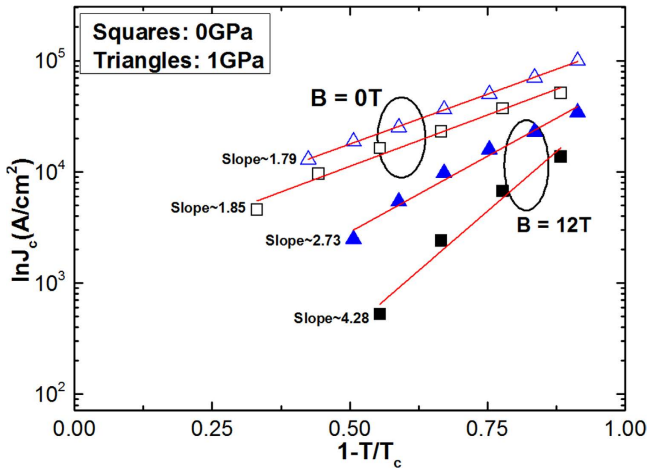

Figure 5. Logarithmic plot of critical current density as a function of reduced temperature at different pressures and magnetic fields.

In Fig. 5, we show the temperature dependence of J_c at 0 and 12 T under different pressures. It follows power law [$J_c \propto (1\text{-}T/T_c)^{\beta}$] behaviour at different pressures. According to the Ginzburg-Landau theory, the exponent β is used to identify different vortex pinning mechanisms at specified fields. It was found that $\beta = 1$ refers to non-interacting vortices and $\beta > 1.5$ corresponds to the core pinning mechanism[26]. The exponent β (i.e. slope of the fitting line) is found to be 1.79 and 1.85 for zero field, and 2.73 and 4.28 at 12 T, at 0 and 1 GPa, respectively, which shows strong J_c dependence on pressure. The low values of β at $P = 1$ GPa indicate that the J_c decays rather slowly in comparison to its values at $P = 0$ GPa. In addition, the differences between $P = 0$ GPa and $P = 1$ GPa scaling show a real pressure effect, the factor is roughly 2, which corresponds nicely to the low-T data in inset Fig. 3.

For polycrystalline bulks, high pressure can modify grain boundaries through reduction of the tunnelling barrier width and the tunnelling barrier height. The Wentzel-Kramers-Brillouin (WKB) approximation applied to a potential barrier gives the following simple expression[36–38]:

$$J_c = J_{co} \exp(-2kW) \quad (1)$$

Where W is the barrier width, $k = (2mL)^{1/2}/\hbar$ is the decay constant, which depends on the barrier height L, $\hbar$; is the Planck constant, and J_{c0} is the critical current density at 0 K and 0T. The relative pressure dependence of J_c can be obtained from Eq. (1) as[39]:

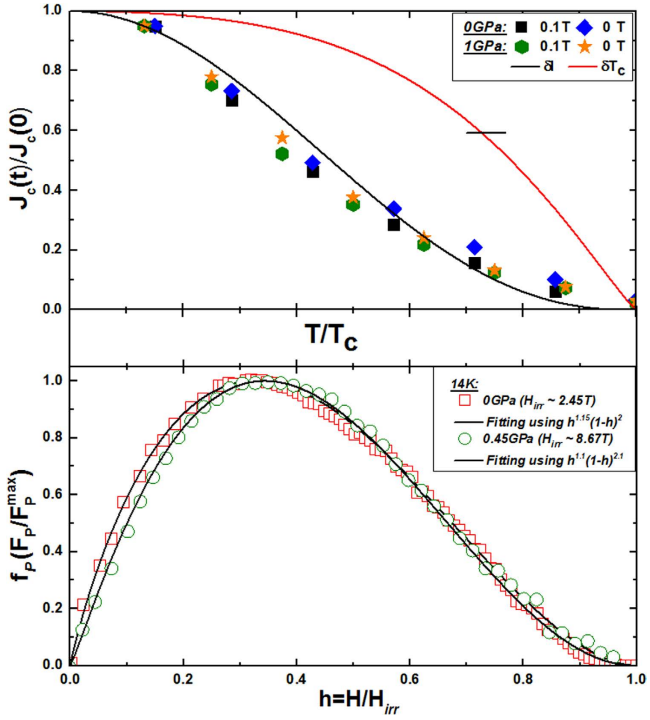

Figure 6. Top panel shows normalized temperature dependence ($t = T/T_c$) of normalized measured J_c at 0.1 T and 0 T, in good agreement with δl pinning. Lower panel shows plots of F_p vs H/H_{irr} at $P = 0$ GPa and $P = 0.45$ GPa at 14 K. The experimental data is fitted through the Dew-Hughes model, and the parameters are given in inset.

$$\frac{d\ \ln\ J_c}{dP} = \frac{d\ \ln\ J_{c0}}{dP} - \left[\left(\frac{d\ \ln\ W}{dP}\right)\ln\left(\frac{J_{c0}}{J_c}\right)\right] - \frac{1}{2}\left[\left(\frac{d\ \ln\ L}{dP}\right)\ln\left(\frac{J_{c0}}{J_c}\right)\right]$$
$$= \frac{d\ \ln\ J_{c0}}{dP} + \kappa_{GB}\ \ln\left(\frac{J_{c0}}{J_c}\right) + \frac{1}{2}\kappa_L\ \ln\left(\frac{J_{c0}}{J_c}\right) \quad (2)$$

Where the compressibility in the width and height of the grain boundary are defined by $\kappa_{GB} = -d\ \ln\ W/dP$ and , respectively. For single crystals, we assume to a first approximation that κ_{GB} and κ_L are roughly comparable, respectively,to the average linear compressibility values $\kappa_a = -d\ln a/dP$ ($\kappa_a \approx -0.029\ \mathrm{GPa}^{-1}$) and $\kappa_c = -d\ln c/dP$ ($\kappa_c \approx -0.065\ \mathrm{GPa}^{-1}$) of $NaFe_{0.97}Co_{0.03}As$ crystal in the FeAs plane, where a and c are the in-plane and out-of-plane lattice parameters, respectively[26]. Therefore, we can write Eq. (2) as

$$\frac{d\ \ln\ J_c}{dP} \sim \frac{d\ \ln\ J_{c0}}{dP} + \kappa_a\ \ln\left(\frac{J_{c0}}{J_c}\right) + \frac{1}{2}\kappa_c\ \ln\left(\frac{J_{c0}}{J_c}\right) \quad (3)$$

By using $J_c \cong 1.3 \times 10^3$ A/cm^2 at 14 K and $J_{c0} \sim 10^5$ A/cm^2, we find that $(\kappa_a\ \ln(J_{co}/J_c)) \approx 0.12\ \mathrm{GPa}^{-1}$ and $(1/2\kappa_c\ \ln(J_{co}/J_c)) \approx 0.14\ \mathrm{GPa}^{-1}$, so that both of them together only contribute less than 10% to the already mentioned experimental value $d\ln J_c/dP = 2.09\ \mathrm{GPa}^{-1}$ inset of Fig. 2b). This result suggests that the origin of the significant increase in $J_c(T)$ under pressure does not arise from the reduction of volume but mainly due to the pressure induced pinning centre phenomenon.

To gain further insight into the pressure effect on the pinning mechanism in $NaFe_{0.97}Co_{0.03}As$, the experimental results have been analysed by using collective pinning theory. There are two predominant mechanisms of core pinning, i.e. $\delta\ell$ pinning, which comes from spatial variation in the charge carrier mean free path,ℓ, and δT_c pinning due to randomly distributed spatial variation in T_c. According to the theoretical approach proposed by Griessen *et al.*[40], $J_c(t)/J_c(o) \propto (1 - t^2)^{5/2}(1 + t^2)^{-1/2}$ in case of $\delta\ell$ pinning, whereas $J_c(t)/J_c(o) \propto (1 - t^2)^{7/6}(1 + t^2)^{5/6}$ corresponds to δT_c pinning, where $t = T/T_c$ Fig. 6 (Top Panel) shows a comparison between the experimental J_c values and the theoretically expected variation within the $\delta\ell$ and δT_c pinning mechanisms at 0.1 T and 0 T (the so-called remanent state shown by the solid symbols). The $J_c(t)$ values have been obtained from the $J_c(B)$ curves at various temperatures.

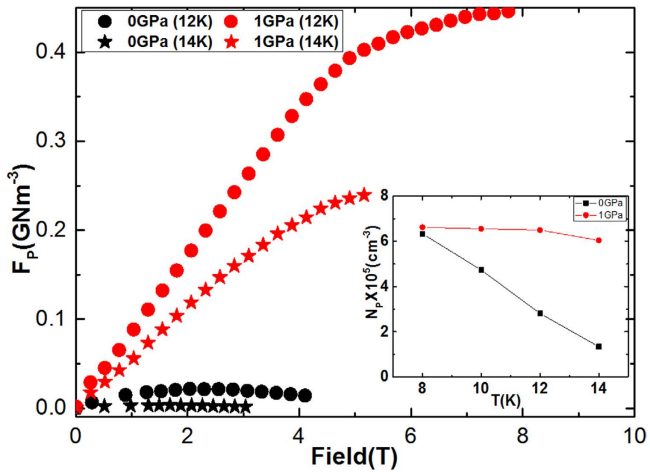

Figure 7. Pinning force density (F_p) as a function of field at $P = 0$ GPa and $P = 1$ GPa at 12 K and 14 K. The inset shows the temperature dependence of the pinning centre number density at the different pressures.

It is found that the experimental data at $P = 0$ and $P = 1$ GPa are in good agreement with theoretical $\delta\ell$ pinning. It is more likely that pinning in $NaFe_{0.97}Co_{0.03}As$ originates from spatial variation of the mean free path "ℓ". We observed similar results in $BaFe_{1.9}Ni_{0.1}As_2$ and $SiCl_4$ doped MgB_2 at low fields. In addition, $\delta\ell$ pinning has also been reported in $FeTe_{0.7}Se_{0.3}$ crystal[41–43]. In order to understand the nature of the pinning mechanisms in more detail, it is useful to study the variation of the vortex pinning force density, with the field. The normalized pinning force density (F_p/F_p^{max}) as a function of reduced field (H/H_{irr}) at $P = 0$ GPa and $P = 0.45$ GPa at 14 K is plotted in lower panel of Fig. 6. H_{irr} is estimated by using the criterion of Jc ~100A/cm^2. We can use the Dew-Hughes formula, i.e. $F_p \propto h^m(1 - h^n)$ to fit our experimental data, where m and n are fitting parameters to describe the nature of the pinning mechanism. We found that $m = 1.15$ and $n = 2$ at 0 GPa, and $m = 1.1$ and $n = 2.1$ at 0.45 GPa. According to the Dew-Hughes model, in the case of $\delta\ell$ pinning for a system dominated just by point pinning, the values of the fitting parameters are $m = 1$ and $n = 2$, with the $F_p^{normalized}$maxima occurring at $h_{max} = 0.33$, while h_{max} occurs at 0.20 for surface/grain boundary pinning with $m = 0.5$ and $n = 2$. In case of δT_c pinning, h_{max} shifts to higher values, and the fitting parameters change accordingly. Further details can be found elsewhere[44]. The values of m and n that were found in the present study are almost the same at 0 GPa and 0.45 GPa, so normal core point pinning is dominant in our material.

Pressure can enhance the pinning force strength by a significant amount in $NaFe_{0.97}Co_{0.03}As$ single crystal. The pinning force density as a function of field at 12 K and 14 K is plotted in Fig. 7. At high field and pressures, the F_p is found to be over 20 and 80 times higher than at 0 GPa at 12 and 14 K, respectively. Furthermore, pressure induces more point pinning centres at 12 K and 14 K, especially at $P = 1$ GPa, as can be seen in the inset of Fig. 7. The number density of randomly distributed effective pinning centres (N_p) can be calculated from the following relation:

$$\frac{\Sigma F_p}{\eta f_p^{max}} = N_{Pp} \tag{4}$$

Where ΣF_P is the aggregated pinning force density, f_p^{max} is the maximum normalized elementary pinning force (f_p), and η is an efficiency factor. The η value is 1 in the case of a plastic lattice, and the η value is otherwise f_p^{max}/B, where B is the bulk modulus of the material[45]. We can assume that $\eta = 1$, as pressure can shrink lattice parameters. The inset of Fig. 7 shows the N_p versus temperature plot at $P = 0$ and $P = 1$ GPa. The N_p values are found to be much greater at 14 K at $P = 1$ GPa as compared to N_p at $P = 0$ GPa (nearly six times as great). It is well known that hydrostatic pressure induces pinning centres which, in turn, leads to huge values of J_c and increase in N_p at P = 1 Gpa is a direct evidence of that[27,46–48]. This is further verified in Fig. 8, which shows the plot of J_c/J_c^{max} versus reduced field (i.e. H/H_{irr}) at $P = 0$ GPa and $P = 1$ GPa for 14 K and $P = 0$ GPa & $P = 0.45$ GPa for 12 K. Obviously, the hump or secondary peak effect observed at high pressures suggests that the J_c enhancement is due to induced pinning centres.

Additionally, we found a pronounced reduction in the superconducting anisotropy at high temperatures, by almost 63% at $P = 1$ GPa. The pressure dependence of the T_c, volume (V) and anisotropy (γ) are interconnected through a relation[49]:.

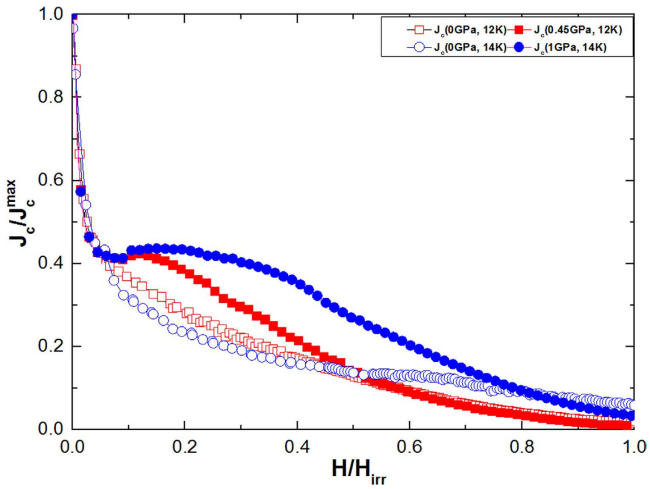

Figure 8. Reduced field dependence of the normalized J_c at 14 K for different pressures. The inset shows the same plot for 12 K at $P = 0$ GPa and $P = 0.45$ GPa.

$$-\left[\frac{T_c^P - T_c^0}{T_c^0}\right] = \left[\frac{\Delta V}{V}\right] + \left[\frac{\gamma_p - \gamma_0}{\gamma_0}\right] \quad (5)$$

At $\Delta P = 1$ GPa, $\Delta V(T_c)/V(T_c)$ is estimated to be –0.02, as $\Delta V/V = -\Delta P/B$, where B is the bulk modulus. We can use the bulk modulus (B≈52.3 GPa) of a similar superconductor, i.e. $Na_{1-x}FeAs$[34]. The value of γ at $P = 1$ GPa is found to be 63% less than its value at $P = 0$ GPa.

Hydrostatic pressure can significantly enhance J_c by up to 10^2 times in $NaFe_{0.97}Co_{0.03}As$ single crystals, which is a record high enhancement. The most significant enhancement in in-field performance of $NaFe_{0.97}Co_{0.03}As$ in terms of pinning force density (F_p) is found at $P = 1$ GPa in particular, where the F_p at high fields is over 20 and 80 times higher at 12 and 14 K, respectively, than at 0 GPa. The hydrostatic pressure induces more effective point pinning centres and N_p at 1 GPa is almost two times higher at 12 K and over six times higher at 14 K compared to the value at 0 GPa. Moreover, a hump or secondary peak effect is found from the plot of the normalized J_c as a function of reduced field. Therefore, this giant enhancement in J_c values for $NaFe_{0.97}Co_{0.03}As$ exists because of more pinning centres induced by pressure and the increase in pinning strength as well. The present study indicates that the supercurrent carrying ability in the Fe111 can be further and significantly increased by the proposed hydrostatic pressure technique. Our results were achived in single crystal samples, which means that the enhancement is intrinsic, and more significant than other reported approaches. It gives us high expections that the tapes or wires made by the same compounds should carry higher supercurrents using the hydrostatic pressure than those at ambient pressure.

Experimental

High-quality single crystals of $NaFe_{0.97}Co_{0.03}As$ have been grown by use of the NaAs flux method. NaAs was obtained by reacting the mixture of the elemental Na and As in anevacuated quartz tube at 200°C for 10 h. Then NaAs, Fe and Co powders were carefully weighed according to the ratio of NaAs:Fe:Co = 4:0.972:0.028, and thoroughly ground. The mixtures were put into alumina crucibles and then sealed in iron crucibles under 1.5 atm of highly pure argon gas. The sealed crucibles were heated to 950°C at a rate of 60 °C/h in the tube furnace filled with the inert atmosphere and kept at 950 °C for 10 h and then cooled slowly to 600 °C at 3 °C/h to grow single crystals.

The temperature dependence of the magnetic moments and the M-H loops at different temperatures and pressures were performed on Quantum Design Physical Property Measurement System (QD PPMS 14 T) by using Vibrating Sample Magnetometer (VSM). We have used HMD High Pressure cell and Daphne 7373 oil as a pressure transmitting medium to apply hydrostatic pressure on a sample. The critical current density was calculated by using the Bean approximation.

References

1. Weiss, J. D. *et al.* High intergrain critical current density in fine-grain $(Ba_{0.6}K_{0.4})Fe_2As_2$ wires and bulks. *Nat. Mater.* **11,** 682; DOI:10.1038/nmat3333 (2012).
2. Ma, Y. Progress in wire fabrication of iron-based superconductors. *Supercond. Sci. Technol.* **25,** 113001; DOI:10.1088/0953-2048/25/11/113001 (2012).
3. Lee, S. *et al.*, Artificially engineered superlattices of pnictide superconductors. *Nat. Mater.* **12**, 392; doi:10.1038/nmat3575 (2013).

4. Si, W. *et al.* High current superconductivity in $FeSe_{0.5}Te_{0.5}$-coated conductors at 30 tesla. *Nat. Commun.* **4,** 1347; DOI:10.1038/ncomms2337 (2013).
5. Fang, L. *et al.* Huge critical current density and tailored superconducting anisotropy in $SmFeAsO_{0.8}F_{0.15}$ by low-density columnar-defect incorporation. *Nat. Commun.* **4,** 2655; DOI:10.1038/ncomms3655 (2013).
6. Fang, L. *et al.* High magnetic field independent critical currents in (Ba,K)Fe_2As_2 crystals. *App. Phys. Lett*. **101,** 012601; DOI:10.1063/1.4731204 (2012).
7. Katase, T., Hiramatsu, H., Kamiya, T. & Hosono, H. High Critical Current Density 4 MA/cm^2 in Co-Doped $BaFe_2As_2$ Epitaxial Films Grown on (La,Sr)(Al,Ta)O_3 Substrates without Buffer Layers. *App. Phys. Express* **3,** 063101; DOI:10.1143/APEX.3.063101 (2010).
8. Moll, P. J. W. *et al.* High magnetic-field scales and critical currents in SmFeAs(O, F) crystals, *Nat. Mater.* **9,** 628; DOI:10.1038nmat2795 (2010).
9. Hunte, F. *et al.* Two-band superconductivity in $LaFeAsO_{0.89}F_{0.11}$ at very high magnetic fields. *Nature* **453,** 903; DOI:10.1038/nature07058 (2008).
10. Jaroszynski, J. *et al.* Upper critical fields and thermally-activated transport of $NdFeAsO_{0.7}F_{0.3}$ single crystal. *Phys. Rev. B* **78,** 174523; DOI: http://dx.doi.org/10.1103/PhysRevB.78.174523 (2008).
11. Rall, D. *et al.* Critical current densities in ultrathin Ba(Fe,Co)As microbridges. *Phys. Rev. B* **83,** 134514; DOI: http://dx.doi.org/10.1103/PhysRevB.83.134514 (2011).
12. Wang, X. L., Ghorbani, S. R., Peleckis, G. & Dou, S. X. Very high critical field and superior J_c-Field Performance in $NdFeAsO_{0.82}F_{0.18}$ with T_c of 51K. *Adv. Mater*. **21,** 236; DOI:10.1002/adma.200801527 (2009).
13. Wang, X. L. *et al.* Very strong intrinsic flux pinning and vortex avalanches in (Ba,K)Fe_2As_2 superconducting single crystals. *Phys. Rev. B* **82,** 024525; DOI:10.1103/PhysRevB.82.024525 (2010).
14. Miura, M. *et al.* Strongly enhanced flux pinning in one-step deposition of $BaFe_2(As_{0.66}P_{0.33})_2$ superconductor films with uniformly dispersed $BaZrO_3$ nanoparticles. *Nat. Commun.* **4,** 2499; DOI: 10.1038/ncomms3499 (2013).
15. Nakajima, Y. *et al.* Enhancement of critical current density in Co-doped $BaFe_2As_2$ with columnar defects introduced by heavy-ion irradiation. *Phys. Rev. B* **80,** 012510; DOI:10.1103/PhysRevB.80.012510 (2009).
16. Wang, J. *et al.* Enhancement of critical current density and flux pinning in oxygen ion-irradiated MgB_2 thin films. Supercond. *Sci. Technol.* **22,** 045020; DOI:10.1088/0953-2048/22/4/045020 (2009).
17. Dou, S. X. *et al.* Enhancement of the critical current density and flux pinning of superconductor by nanoparticle SiC doping. *App. Phys. Lett.* **81,** 3419; DOI:10.1063/1.1517398 (2002).
18. Wang, L. *et al.* Textured $Sr_{1-x}K_xFe_2As_2$ superconducting tapes with high critical current density. *Physica C* **471,** 1689; DOI:10.1016/j.physc.2011.09.003 (2011).
19. Kihlstrom, K. J. *et al.* High-field critical current enhancement by irradiation induced correlated and random defects in $(Ba_{0.6}K_{0.4})Fe_2As_2$. *App. Phys. Lett.* **103** 202601; DOI:10.1063/1.4829524 (2013).
20. Takahashi, M. & Kumakura, H. Improvement of the J_c–B property of MgB_2 tapes using the Taguchi method. *Supercond. Sci. Technol.* **25,** 115021; DOI:10.1088/0953-2048/25/11/115021 (2012).
21. Pietosa, J. *et al.* Pressure-induced enhancement of the superconducting properties of single-crystalline $FeTe_{0.5}Se_{0.5}$. *J. Phys.: Condens. Matter* **24,** 265701; DOI:10.1088/0953-8984/24/26/265701 (2012).
22. Takahashi, M. & Kumakura, H. The enhancement of critical current density of powder-in-tube processed MgB_2 tapes by pre-heating of Mg and B mixed powder. *Supercond. Sci. Technol.* **26,** 075007; DOI:10.1088/0953-2048/26/7/075007 (2013).
23. Yi, W. *et al.*, High-pressure study on $LaFeAs(O_{1-x}F_x)$ and $LaFeAsO_\delta$ with different T_c. *EPL* **84,** 67009; DOI:10.1209/0295-5075/84/67009 (2008).
24. Ahilan, K. *et al.* Pressure effects on the electron-doped high T_c superconductor $BaFe_2$_xCoxAs2. *J. Phys.: Condens. Matter* **20,** 472201; DOI:10.1088/0953-8984/20/47/472201 (2008).
25. Wang, A. F. *et al.* Pressure effects on the superconducting properties of single-crystalline Co doped NaFeAs. *New J. Phys.* **14,** 113043; DOI:10.1088/1367-2630/14/11/113043 (2012)
26. Margadonna, S. *et al.* Pressure evolution of the low-temperature crystal structure and bonding of the superconductor FeSe (T_c = 37 K). *Phys. Rev. B* **80,** 064506; DOI:10.1103/PhysRevB.80.064506 (2009)
27. Shabbir, B. *et al.* Hydrostatic pressure: A very effective approach to significantly enhance critical current density in granular $Sr_4V_2O_6Fe_2As_2$ superconductor. *Sci. Rep.* **5,** 8213; DOI: 10.1038/srep08213 (2015).
28. Shlyk, L., Bischoff, M., Rose, E. & Niewa, R. Flux pinning and magnetic relaxation in Ga-doped LiFeAs single crystals. *J. App. Phys.* **112,** 053914; DOI:10.1063/1.4749804 (2012).
29. Chen, G. F., Hu, W. Z., Luo, J. L. & Wang, N. L. Multiple Phase Transitions in Single-Crystalline $Na_{1-\delta}FeAs$. *Phys. Rev. Lett.* **102,** 227004; DOI:10.1103/PhysRevLett.102.227004 (2009).
30. Wang A. F. *et al.* Phase diagram and calorimetric properties of NaFeCoAs. *Phys. Rev. B* 85, 224521; DOI: 10.1103/PhysRevB.85.224521 (2012).
31. Parker, D. R. *et al.* Control of the Competition between a Magnetic Phase and a Superconducting Phase in Cobalt-Doped and Nickel-Doped NaFeAs using electron count. *Phys. Rev. Lett.* **104,** 057007; DOI: 10.1103/PhysRevLett.104.057007 (2010).
32. Wright, J. D. *et al.* Gradual destruction of magnetism in the superconducting family $NaFe_{1-x}Co_xAs$. *Phys. Rev. B* **85,** 054503; DOI: 10.1103/PhysRevB.85.054503 (2012).
33. Medvedev, S. *et al.* Electronic and magnetic phase diagram of β-$Fe_{1.01}Se$ with superconductivity at 36.7 K under pressure. *Nat. Mater*. **8,** 630 DOI:10.1038/nmat2491 (2009).
34. Liu, Q. *et al.* Pressure-Induced Isostructural Phase Transition and Correlation of FeAs Coordination with the Superconducting Properties of 111-Type $Na_{1-x}FeAs$. *J. Am. Chem. Soc.* **133,** 7892; DOI:10.1021/ja2009949 (2011).
35. Bud'ko, S. L., Davis, M. F., Wolfe, J. C., Chu, C. W. & Hor, P. H. Pressure and temperature dependence of the critical current density in $YBa_2Cu_3O_{7-\delta}$ thin films. *Phys. Rev. B* **47,** 2835; DOI: 10.1103/PhysRevB.47.2835 (1993).
36. Halbritter, J. Pair weakening and tunnel channels at cuprate interfaces. *Phys. Rev. B* **46,** 14861; DOI: 0.1103/PhysRevB.46.14861 (1992).
37. Tomita, T., Schilling, J. S., Chen, L., Veal, B. W. & Claus, H. Pressure-induced enhancement of the critical current density in superconducting $YBa_2Cu_3O_x$ bicrystalline rings. *Phys. Rev. B* **74,** 064517; DOI:10.1103/PhysRevB.74.064517 (2006).
38. Browning, N. D. *et al.* The atomic origins of reduced critical currents at [001] tilt grain boundaries in $YBa_2Cu_3O_{7-\delta}$ thin films. *Physica C* **294,** 183; DOI: 10.1016/S0921-4534(97)01689-4 (1998).
39. Tomita, T., Schilling, J. S., Chen, L., Veal, B. W. & Claus, H. Enhancement of the Critical Current Density of $YBa_2Cu_3O_x$ Superconductors under Hydrostatic Pressure. *Phys. Rev. Lett.* **96,** 077001; DOI:10.1103/PhysRevLett.96.077001 (2006).
40. Griessen, R. *et al.* Evidence for mean free path fluctuation induced pinning in $YBa_2Cu_3O_7$ and $YBa_2Cu_4O_8$ films. *Phys. Rev. Lett.* **72,** 1910; DOI: 10.1103/PhysRevLett.72.1910 (1994).
41. Shahbazi, M., Wang, X. L., Choi, K. Y. & Dou, S. X. Flux pinning mechanism in $BaFe_{1.9}Ni_{0.1}As_2$ single crystals: Evidence for fluctuation in mean free path induced pinning. *Appl. Phys. Lett.* **103,** 032605; DOI:10.1063/1.4813113 (2013).
42. Bonura, M., Giannini, E., Viennois, R. & Senatore, C. Temperature and time scaling of the peak-effect vortex configuration in $FeTe_{0.7}Se_{0.3}$. *Phys. Rev. B* **85,** 134532; DOI:10.1103/PhysRevB.85.134532 (2012).

43. Wang, X. L. *et al.* Enhancement of the in-field *Jc* of MgB_2 via $SiCl_4$ doping. *Phys. Rev. B* **81,** 224514; DOI:10.1103/PhysRevB.81.224514 (2010).
44. Dew-Hughes, D. Flux pinning mechanisms in type II superconductors. *Phil. Mag.* **30,** 293; DOI:10.1080/14786439808206556 (1974).
45. Colliongs, E. W. *A*pplied Superconductivity: Metallurgy, and Physics of Titanium Alloys Vol. **2**: Applications. Springer N. Y. (1986).
46. Kuklja, M. M. & Kunz, A. B. Ab initio simulation of defects in energetic materials: Hydrostaticcompression of cyclotrimethylene trinitramine. *J. App. Phys.* **86,** 4428; DOI:10.1063/1.371381 (1999).
47. Londos, C. A., Potsidi, M. S., Bak-Misiuk, J., Misiuk, A. & Emtsev, V. V. Pressure assisted evolutionof defects in silicon. *Cryst. Res. Technol.* **38,** 1058; DOI:10.1002/crat.200310136 (2003).
48. Misiuk, A. Evolution of Process - Induced Defects in Silicon under Hydrostatic Pressure. *Solid State Phenomena* **19-20,** 387–392; DOI:10.4028/SSP.19-20.387 (1991).
49. Schneider, T. & Castro, D. D. Pressure and isotope effect on the anisotropy of MgB_2. *Phys. Rev. B* **72,** 054501; DOI:10.1103/PhysRevB.72.054501 (2005).

Acknowledgments

X.L.W. acknowledges the support from the Australian Research Council (ARC) through an ARC Discovery Project (DP130102956) and an ARC Professorial Future Fellowship project (FT130100778).

Author Contributions

X.L.W. conceived the pressure effects and designed the experiments. B.S. performed high pressure measurements. X.H.C. and A.F.W. provided samples. X.L.W. and B.S. analysed the data and wrote the paper. S.R.G. and S.D. contributed to the discussions of the data and the paper.

Additional Information

Competing financial interests: The authors declare no competing financial interests.

How to cite this article: Shabbir, B. *et al.* Giant enhancement in critical current density, up to a hundredfold, in superconducting $NaFe_{0.97}Co_{0.03}$ As single crystals under hydrostatic pressure. *Sci. Rep.* **5**, 10606; doi: 10.1038/srep10606 (2015).